

Electronic Supplementary Information

A Rationally Assembled Graphene Nanoribbon/Graphene Framework for High Volumetric Energy and Power Density Li-Ion Batteries

Liangliang Gao^a, Yi Jin^b, Xiaofang Liu^a, Ming Xu^c, Xiaokang Lai^b, Jianglan Shui*^a

^a School of Materials Science and Engineering, Beihang University, Beijing 100083, China

^b State Key Laboratory of Operation and Control of Renewable Energy & Storage Systems, China
Electric Power Research Institute, Beijing 100192, China

^c School of Materials Science and Engineering, Huazhong University of Science and Technology,
Wuhan 430074, China.

*Corresponding author: Jianglan Shui

E-mail: shuijianglan@buaa.edu.cn

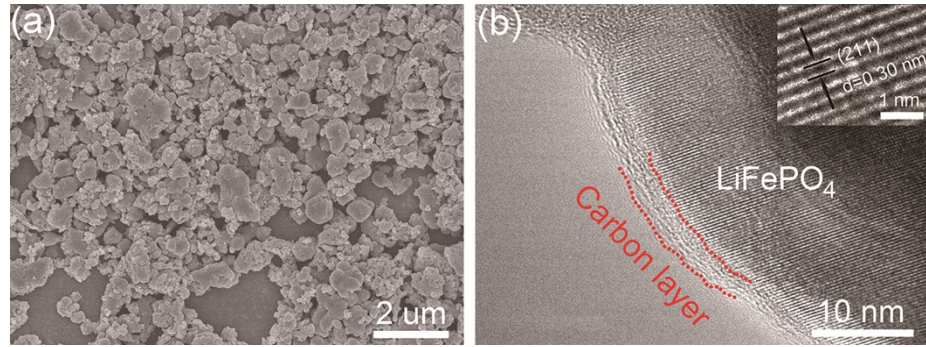


Fig. S1 (a) SEM and (b) TEM images of commercial LiFePO₄ used in this work.

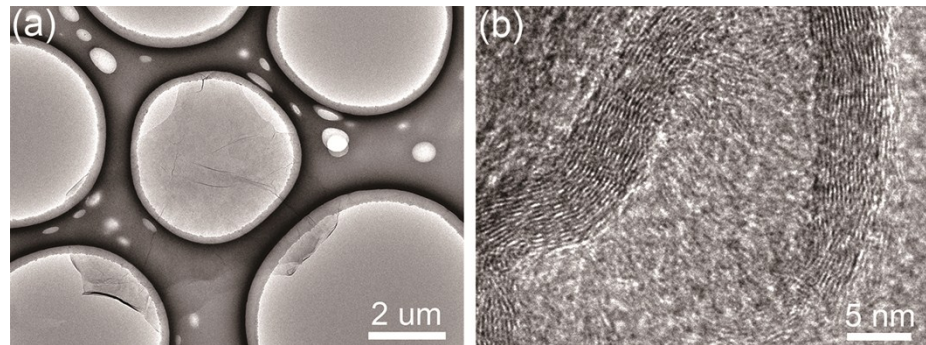


Fig. S2 (a) TEM image of a single piece of GO; (b) HRTEM image of the edges of reduced graphene oxide (rGO) showing 15~20 layers of graphene.

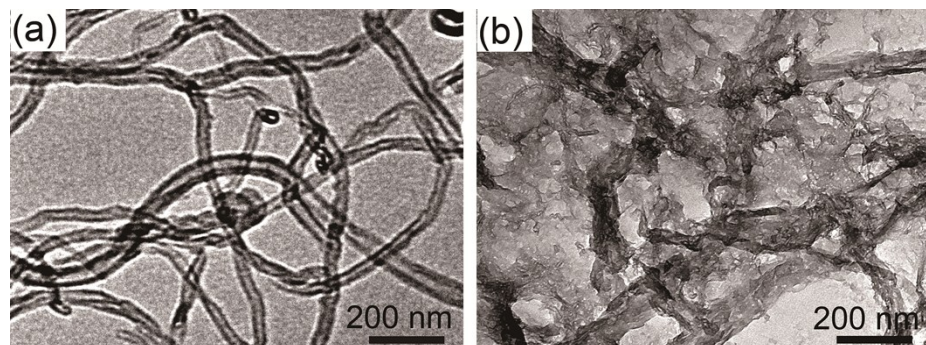


Fig. S3 TEM images of (a) CNT precursor (diameter ~50 nm) as well as resultant (b) GONR (width ~150 nm) obtained by a chemical oxidation method.¹

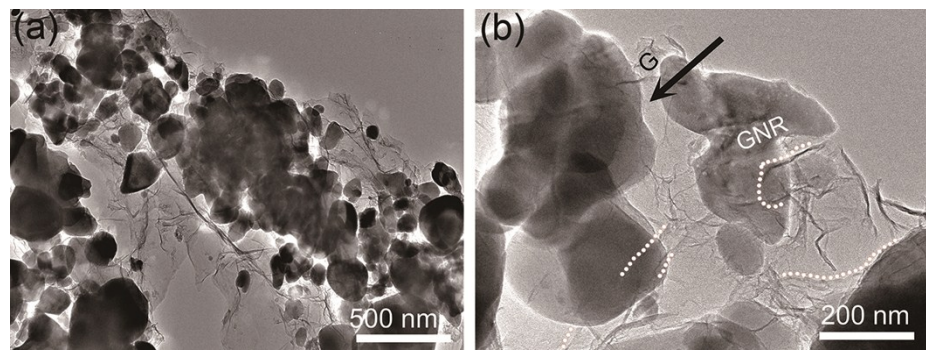


Fig. S4 TEM images of LFP/GNR/G sample. White dot lines in (b) outline some GNRs which bridge LFP particles and G sheets.

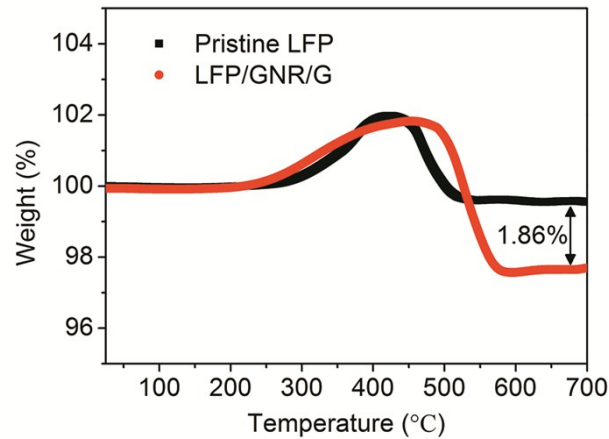


Fig. S5 Thermogravimetric curves of pristine LFP and LFP/GNR/G. The GNR/G content in LFP/GNR/R was 1.86%, which confirmed the result of 2% in Table S2.

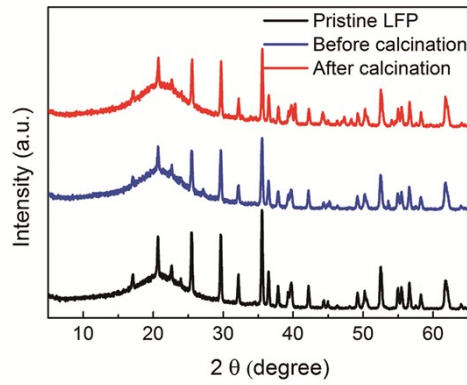


Fig. S6 XRD patterns of commercial LFP, as well as LFP/GNR/G sample before and after a calcination at 600 °C in Ar/H₂(90/10, V/V) for 5 h.

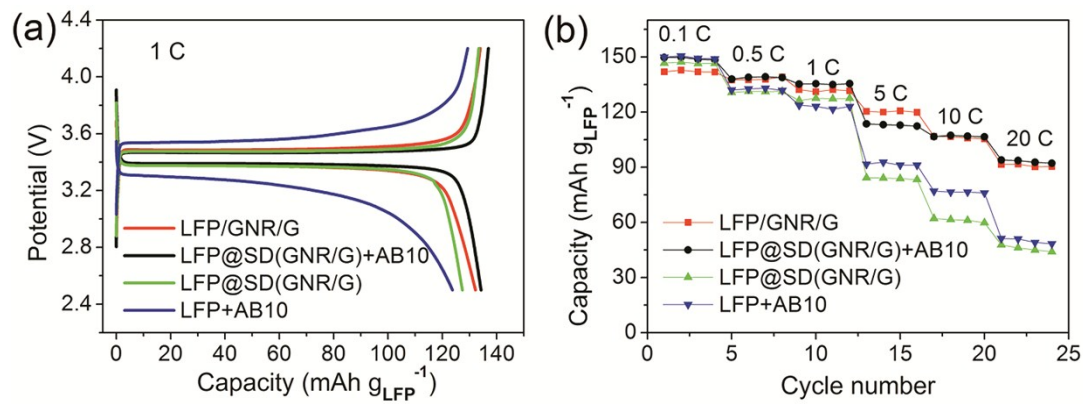


Fig. S7 Comparison of (a) charge/discharge curves at the current rate of 1 C, and (b) rate capabilities of LFP+AB10, LFP@SD(GNR/G), LFP@SD(GNR/G)+AB10 and LFP/GNR/G based on the commercial LFP weight only.

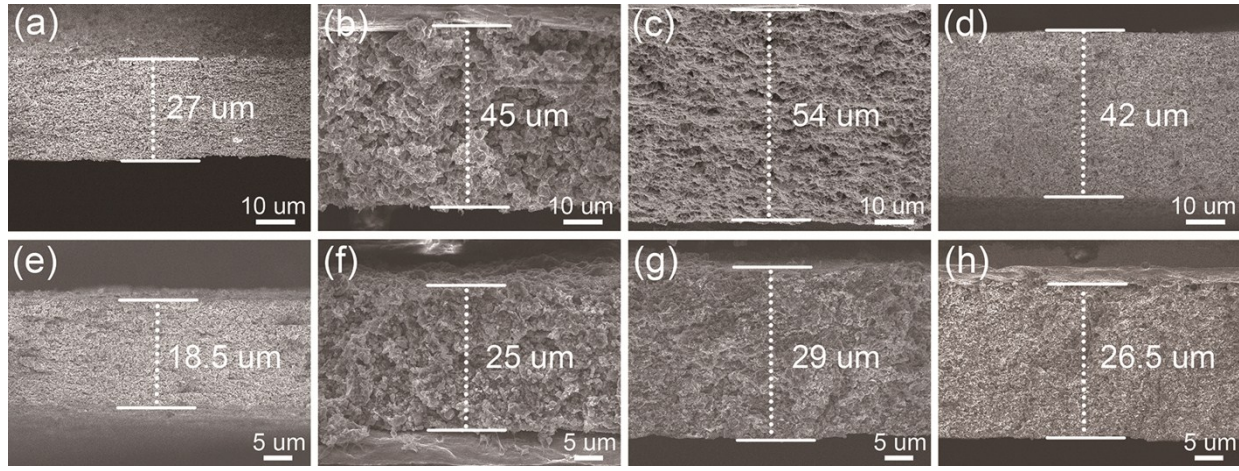


Fig. S8 Cross-sectional SEM images of four electrode samples with electrode weight of 5 mg cm^{-2} (including active material, conductive additive and binder) before and after compression under a pressure of 50 MPa: (a, e) LFP/GNR/G; (b, f) LFP@SD(GNR/G); (c, g) LFP@SD(GNR/G)+AB10; (d, h) LFP+AB10.

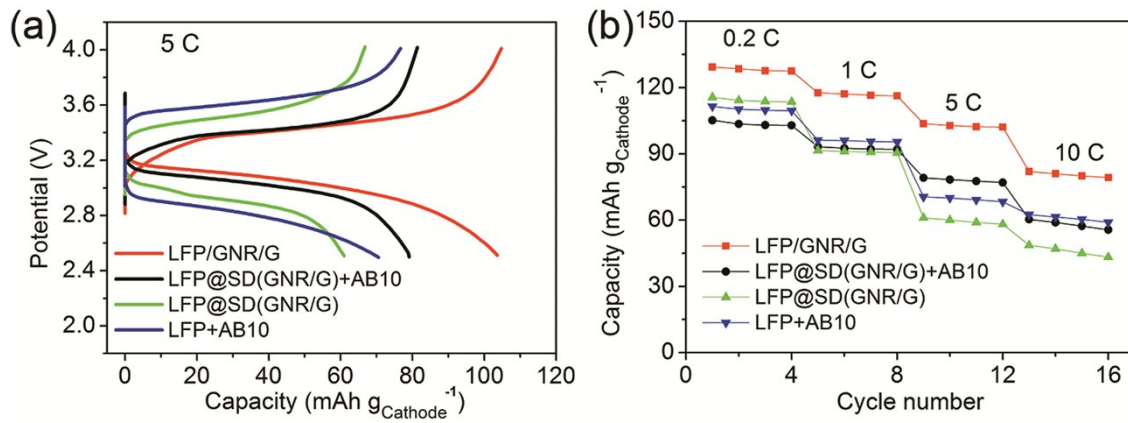


Fig. S9 Comparison of electrodes LFP+AB10, LFP@SD(GNR/G)+AB10, LFP@SD(GNR/G) and LFP/GNR/G based on the cathode weight in full cells with graphite as the anode material. (a) Charge/discharge curves at the current rate of 5 C and (b) rate capabilities.

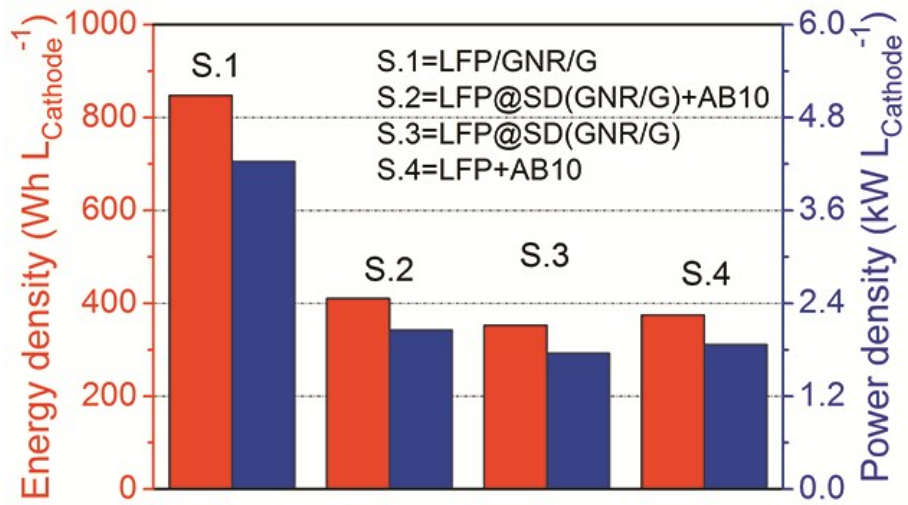


Fig. S10 Energy density and power density comparisons of LFP+AB10, LFP@SD(GNR/G)+AB10, LFP@SD(GNR/G) and LFP/GNR/G samples in full cells at 5 C rate. The discharge median-potentials of 2.81 V, 2.91 V, 3.02 V and 3.03 V were used for LFP+AB10, LFP@SD(GNR/G), LFP@SD(GNR/G)+AB10 and LFP/GNR/G samples, respectively.

Table S1 EDS elemental analysis of commercial LiFePO₄.

| Element | Mass% | Atomic% |
|-----------------|--------|---------|
| C _K | 8.16 | 14.54 |
| O _K | 46.79 | 62.57 |
| P _K | 18.32 | 12.65 |
| Fe _K | 26.73 | 10.24 |
| Total amount | 100.00 | 100.00 |

Table S2 The residual contents of freeze-dried GO and GONR after 600 °C treatment in Ar/H₂ (90/10, V/V) for 5 h.

| Samples | Freeze-dried GO sponge | Freeze-dried GONR sponge |
|-------------------------------|------------------------|--------------------------|
| Mass before calcinations [mg] | 28.27 | 14.53 |
| Mass after calcinations [mg] | 11.35 | 5.98 |
| Residual content [%] | 40.1 | 41.2 |

Table S3 Specific capacity comparison of reported LFP electrodes.

| Size [nm] / morphology of LFP | Resource of LFP | With Polym -eric binder or not | Conductive additives | | Specific properties at 5 C rate (current collector excluded) | | | Ref. |
|--------------------------------------|---|--|---|--------------------|---|---|---|----------------------|
| | | | Material | Content [wt.%] | Gravimetric capacity [mAh g ⁻¹] | Volumetric capacity [mAh cm ⁻³] | Volumetric energy density [Wh L ⁻¹] | |
| 100 – 2000 (particles) | Commercial | N | G, GNR | 1.0, 1.0 | 118 | 318 | 1020 | This work |
| 100 – 800 (particles) | Commercial | N | G | 7.5 | 98.5 | | | 2 |
| 140 (particles) | Commercial | Y | Carbon black | 5 | ~145 | ~260 | ~850 | 3 |
| 3000 – 7000 (porous particles) | Hydrothermal | Y | Carbon black | 15 | ~100 | ~150 | ~500 | 4 |
| D=30 – 100 L=80 – 400 (rods) | Hydrothermal | Y | G, Carbon black | <0.7, 8 | ~105 | | | 5 |
| 4000 – 6000 (porous particles) | Hydrothermal and chemical lithiation | Y | CNT, Carbon black | ~1.2, 10 | ~95 | ~150 | ~500 | 6 |
| ~40 (particles) | Hydrothermal | Y | CNT, Carbon black | ~2.2, ~12.8 | ~95 | | | 7 |
| D=20 L=100 (rods) | Hydrothermal | Y | N-doped carbon, G, Carbon black | ~1.6, ~2, 10 | ~126 | ~180 | ~600 | 8 |
| ~50 – 200 (particles) | Precipitation and chemical lithiation | Y | N-doped G | ~11.4 | ~125 | <200 | ~650 | 9 |
| ~100 (particles) | Hydrothermal | Y | G, Carbon black | 3.6, 10 | ~84 | | | 10 |

^{a)}Y: Yes; ^{b)}N: No; ^{c)}G: Graphene

References

- 1 C. Wang, Y.S. Li, J. Jiang, W.H. Chiang, *ACS Appl. Mater. Interfaces*, 2015, **7**, 17441-17449.
- 2 Y. Huang, H. Liu, Y.-C. Lu, Y. Hou, Q. Li, *J. Power Sources*, 2015, **284**, 236-244.
- 3 D.P. Singh, F.M. Mulder, A.M. Abdelkader, M. Wagemaker, *Adv. Energy Mater.*, 2013, **3**, 572-578.
- 4 M.-Y. Cho, H. Kim, H. Kim, Y.S. Lim, K.-B. Kim, J.-W. Lee, K. Kang, K.C. Roh, *J. Mater. Chem. A*, 2014, **2**, 5922-5927.
- 5 Y. Long, Y. Shu, X. Ma, M. Ye, *Electrochim. Acta*, 2014, **117**, 105-112.
- 6 M. Chen, C. Du, B. Song, K. Xiong, G. Yin, P. Zuo, X. Cheng, *J. Power Sources*, 2013, **223**, 100-106.
- 7 B. Wang, T. Liu, A. Liu, G. Liu, L. Wang, T. Gao, D. Wang, X.S. Zhao, *Adv. Energy Mater.*, 2016, **6**, 1600426.
- 8 K. Zhang, J.T. Lee, P. Li, B. Kang, J.H. Kim, G.R. Yi, J.H. Park, *Nano Lett.*, 2015, **15**, 6756-6763.
- 9 J.-P. Jegal, K.-C. Kim, M.S. Kim, K.-B. Kim, *J. Mater. Chem. A*, 2014, **2**, 9594-9599.
- 10 W.-B. Luo, S.-L. Chou, Y.-C. Zhai, H.-K. Liu, *J. Mater. Chem. A*, 2014, **2**, 4927-4931.